Romanian Reports in Physics **70**, 405 (2018)

SILICON MICRORING WITHIN A FIBER LASER CAVITY FOR HIGH-REPETITION-RATE PULSE TRAIN GENERATION

M. MEISTERHANS[1], A. COILLET[1,*], F. AMRANI[1,2], O. DEMICHEL[1], J.-B. JAGER[3], P. NOÉ[4], J.-M. FÉDÉLI[4], F. DE FORNEL[1], PH. GRELU[1,a], B. CLUZEL[1,b]

[1]Laboratoire Interdisciplinaire Carnot de Bourgogne UMR CNRS 6303, Université de Bourgogne Franche-Comté, 9 avenue A. Savary, BP 47870, 21078 Dijon, France
[2]Laboratoire XLIM UMR 7252 CNRS, Université de Limoges, 123, avenue Albert Thomas, 87060 Limoges, France
[3]Université Grenoble Alpes, F-38000 Grenoble, France, CEA INAC, MINATEC Campus, F-38054 Grenoble, France
[4]Université Grenoble Alpes, F-38000 Grenoble, France, CEA LETI, MINATEC Campus, F-38054 Grenoble, France
Emails: [a] philippe.grelu@u-bourgogne.fr, [b] benoit.cluzel@u-bourgogne.fr
[*]Corresponding Author, Email: aurelien.coillet@u-bourgogne.fr

Received September 25, 2017

Abstract. We investigate the generation of trains of short optical pulses whose repetition frequency is imposed by the free spectral range of a silicon microring resonator embedded into a fiber laser cavity. According to the microresonator selected in a silicon-on-insulator chip, the pulse trains are obtained with repetition frequencies ranging from 110 GHz to 450 GHz. Regimes where multiple pulses are generated in the microresonator are also shown, and nonlinear broadening of the laser lines is observed.

Key words: fiber lasers, mode-locked lasers, silicon photonics, optical resonators.

1. INTRODUCTION

The development of ultrashort pulse sources operating at high repetition rates is driven by diverse applications, ranging from optical communication and signal processing to frequency comb and terahertz generation for sensing, spectroscopy, and metrology [1–3]. To generate pulses at repetition frequencies (RFs) above 100 GHz, the natural scaling inclines toward very short cavities, such as semi-conductor quantum-dot lasers [4]. However, the convenient and versatile fiber laser platform is also amenable to similar RFs through the use of a pulse multiplication mechanism. If we exclude active modulation [5], which is limited by the speed of the driving electronics, passive multiplication techniques appear very promising, as they potentially accomodate the up-scaling of both the RF and the optical power. In passive harmonic mode locking, the RF globally scales linearly with the pumping power P [6], and ultrashort pulse generation at RF exceeding 20 GHz was demonstrated [7].

Modulation instability (MI) is a nonlinear process where the RF scales with $\sqrt{P}$ in passive fibers, and reaches the 100 GHz to THz range [8]. However, the previous passive schemes lack a precise control of the RF, resulting in a poor stability of the pulsed source. By embedding a short cavity inside of the long fiber laser cavity, the RF can be controlled. In 1997, Yoshida *et al.* inserted a Fabry-Perot filter in a MI fiber laser cavity [9]: the free spectral range (FSR) of the Fabry-Perot fixed the RF to 115 GHz; however, the pulsed laser was poorly stable.

Since then, lasers of increasing performance have been demonstrated using variants of this method. A fiber-integrated Mach-Zehnder (MZ) interferometer was shown to control the fiber laser RF over two orders of magnitude [10]. However, the low spectral selectivity of the MZ interferometer results in a poor suppression of supermodal noise, which entails an unstable pulse train generation, as was recently investigated [11]. Thus, it appears essential to incorporate a highly-selective filter element in the fiber laser architecture. In 2012, Peccianti *et al.* demonstrated the first fiber laser harmonically mode-locked by a integrated high-finesse microresonator [12, 13]. The doped-silica, on-chip microresonator provided both high spectral selectivity and nonlinearity, thus promoting the dynamics pulsed at 200 GHz of the whole fiber cavity. By using a silicon microring resonator (SMRR), this approach lead to the recent realization of a 110 GHz-RF mode-locked fiber laser [14, 15]. Working with silicon takes advantage of the huge investment and experience from the microelectronics industry, and contributes to the development of a monolithic platform for optoelectronics [16]. Silicon photonics already offers a large number of ultra-compact, high-performance photonic components [17]. The high Kerr nonlinearity of silicon is instrumental to induce mode locking with a low pumping threshold. However, at the main telecom wavelength (1.55 μm), two-photon-absorption (TPA), free-carriers dispersion (FCD) and their thermalization have to be considered [18], and can be detrimental to formation of the targeted ultrafast dynamics.

In this article, we study the high-repetition-rate short-pulse generation of a fiber laser whose dynamics is driven by an on-chip SMRR. Several SMRRs are tested and coupled into the fiber laser cavity. Beyond showing that the RF effectively corresponds to the FSR of the SMRR, we precise the role of the latter by using polarization-maintaining (PM) fibers in the main cavity length, thus avoiding the interplay of nonlinear polarization evolution in the pulse formation [19]. We discuss the main physical mechanisms at play in the pulsed laser system.

2. LASER ARCHITECTURE

The hybrid fiber-SMRR laser is a unidirectional ring laser composed of a 20-meter-long polarization-maintaining erbium-doped fiber amplifier (PM-EDFA) with

an output saturation power of 27 dBm, an optical isolator followed by a 90/10 output coupler, a SMRR that can be selected on the silicon-on-insulator (SOI) chip, two polarization controllers (PCs) from either side of the SMRR, and a fibered polarization beam splitter (PBS). Since the coupling to and from the SMRR is strongly polarization-dependent, and is performed with short lengths of standard (non-PM) fibers, the PCs are essential. The input PC setting allows to optimize the light coupling into the SMRR. After the SMRR output, the PBS selects the appropriate polarization to input the PM-EDFA, as well as to provide an output coupling on the orthogonal polarization state. Hence, the output coupling ratio, as well as linear cavity losses, are determined by the output PC settings. The experimental setup is sketched in Fig. 1 (a).

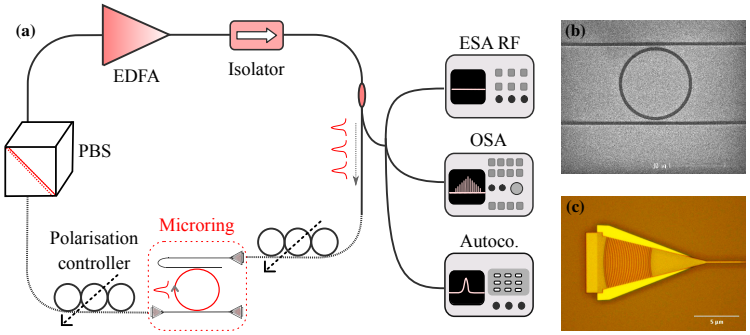

Fig. 1 – (a) Hybrid architecture based on a nonlinear silicon microring embedded into a fiber laser. PM-EDFA: polarization-maintaining erbium-doped fiber amplifier. PBS: polarizing beam-splitter. Microring: silicon-on-insulator optical ring waveguide. (b) Electronic microscope photography of a 10 μm diameter microring. (c) Grating coupler used to couple light from the fiber to the silicon waveguide.

Figure 1 (b) shows the key component of the laser, a microring resonator based on a SOI waveguide. The photonics waveguides are 500 nm-wide and 220 nm-thick, and buried under 2 μm silica [20]. An efficient coupling between a standard silica single-mode optical fiber (SMF) and the integrated SOI circuits is performed using grating couplers, see Fig. 1 (c) [21]. We measured typical coupling losses of 3 dB between the SMF and the transverse-electric (TE) polarization mode on the SOI chip. Using straight guides of various length and identical grating couplers, we calculated the propagation losses to be 3 dB/cm, a value comparable to the state-of-the-art [17]. Light is sent from the input waveguide to the resonator *via* evanescent coupling, and the signal from the drop port is extracted using the same coupling method. Q-factors ranging from 10 000 to 80 000 were measured on SMRRs of diameters 20, 50, 100, and 200 μm. All things considered, the adjunction of the on-chip SMRR

to the fiber loop cavity adds less than 10 dB of losses, which is easily compensated by the large gain of the PM-EDFA. The group-velocity dispersion of the waveguides was simulated using an eigenmode expansion method, and experimentally measured using a Mach-Zehnder interferometer including a straight SOI waveguide on one arm [22]. The numerical simulation yields an anomalous chromatic dispersion of $\beta_2 = -0.28\ \mathrm{ps}^2/\mathrm{m}$ for the waveguide at the operating wavelength 1.55 μm, in good agreement with the experimentally measured dispersion of $-0.31\ \mathrm{ps}^2/\mathrm{m}$. We evalu-

Table 1

Physical quantities used to solve the generalized nonlinear Schrödinger equation in the SOI waveguide

Physical quantity	Value	Reference
$\beta_{2_{\mathrm{exp}}}$	$-0.28\,\mathrm{ps}^2\mathrm{m}^{-1}$	this work
$\beta_{2_{\mathrm{th}}}$	$-0.31\,\mathrm{ps}^2\mathrm{m}^{-1}$	this work
γ_{K}	380 $\mathrm{W}^{-1}\mathrm{m}^{-1}$	this work
γ_{K}	275 $\mathrm{W}^{-1}\mathrm{m}^{-1}$	[23]
β_{TPA}	$5 \times 10^{-12}\,\mathrm{mW}^{-1}$	[23]
τ_{eff}	5 ns	[24, 25]
μ	7.5	[26]
σ	$1.45 \times 10^{-21}\,\mathrm{m}^2$	[27]

ated the effective nonlinearity of the SOI waveguide through the measurement of the spectral broadening of a 10 ps pulsed laser source [28]. While most of the broadening is due to self-phase-modulation (SPM), two-photon absorption and free-carrier effects have to be taken into account to correctly evaluate the effective nonlinearity of our waveguide. TPA strength β_{TPA}, free carrier absorption σ, dispersion μ, and lifetime τ_{eff}, which were not directly accessible from our characterization experiment, were extracted from references [23–27, 29]. The nonlinear propagation of the pulse in the waveguide can be modelled by the following generalized nonlinear Schrödinger envelope equation:

$$\frac{\partial A(z,t)}{\partial z} = \left(-\frac{\alpha_0}{2} - i\frac{\beta_2}{2}\frac{\partial^2}{\partial t^2}\right)A(z,t) + \left(i\frac{\gamma_K}{2} - \frac{\beta_{\mathrm{TPA}}}{2A_{\mathrm{eff}}}\right)|A(z,t)|^2 A(z,t) + \left(\frac{\sigma}{2}(1+i\mu)\frac{\beta_{\mathrm{TPA}}}{2\hbar\omega_0 A_{\mathrm{eff}}^2}e^{(-\frac{t}{\tau_{\mathrm{eff}}})}\right)A^5(z,t) \quad (1)$$

where $A(z,t)$ is the complex electric field envelope amplitude, with z and t being the propagation length and time variables, respectively, α_0 the linear losses measured at 3 dB/cm, A_{eff} the effective area of the mode, and ω_0 the angular frequency of the electromagnetic wave. Performing numerical simulation of this equation using a split-step Fourier algorithm and adjusting the value of the effective nonlinearity γ_K to match the experimental spectrum yields a value of $\gamma_K = 380\ \mathrm{W}^{-1}\mathrm{m}^{-1}$, a value that agrees reasonably well with the literature (275 $\mathrm{W}^{-1}\mathrm{m}^{-1}$ in [23]). These

characterization results are listed up in Table 1.

3. RESULTS AND DISCUSSION

Figure 2 shows the recorded spectra at the output of the fiber laser using each microring as the mode-locking element. Laser emission is obtained and comprises several frequency comb lines when the output power of the amplifier is typically greater than 20 dBm. The lasing regimes shown in Fig. 2 are obtained for broad and reproducible ranges of the positions of the PCs. As expected, the interval between the comb lines matches the FSR of the microring, and increases when the diameter of the ring resonator is decreased. For a diameter of 20 μm, the FSR is so large that only three lines can be excited within the PM-EDFA gain bandwidth.

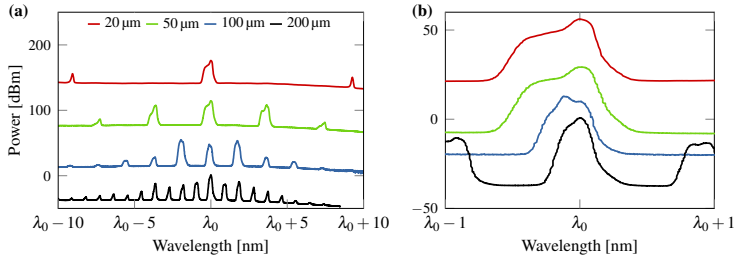

Fig. 2 – Measured optical spectra at the laser output for 50, 100, and 200 μm-diameter microring resonators. Several modes of the microresonator are lasing for a pump power of 27 dBm, and nonlinear broadening of these modes is occurring. (b) A zoom on the central mode shows that the smaller the diameter, the broader the spectral line.

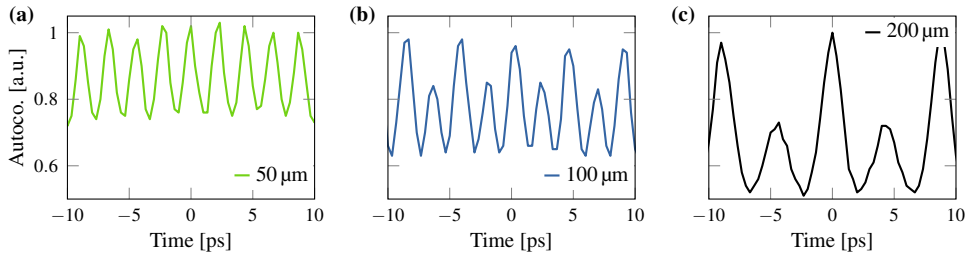

Fig. 3 – Autocorrelation traces for the (a) 50, (b) 100, and (c) 200 μm-diameter microring resonators. In each case pulses are obtained, confirming the mode-locking of the cavity. The repetition rates are compatible with the FSR of each microring resonator, suggesting that it is responsible for the mode-locking of the whole fiber cavity.

A multi-shot intensimetric autocorrelator of the second order is used to determine the average short-pulse pattern, and assess its stability, in order to compare the

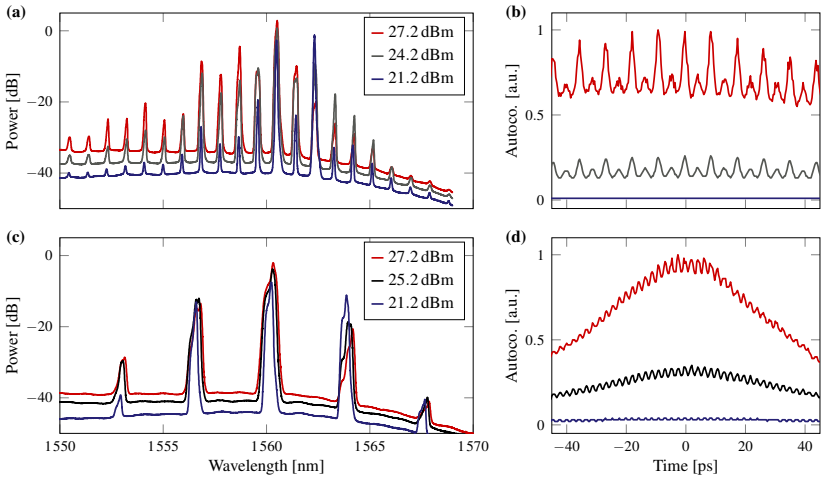

Fig. 4 – Spectrum (a) and autocorrelation traces (b) for the fiber laser with the 200 μm-diameter SMRR compared to the 50 μm-diameter case (c) and (d). In both cases, increasing the pump power leads to higher coherence and contrast.

obtained dynamics with the harmonic mode-locking of the long fiber laser cavity [7, 11]. Figure 3 demonstrates the existence of short pulsations that are obtained at a main RF of 113 GHz, 227 GHz, and 450 GHz for SMRR diameters of 200 μm, 100 μm, and 50 μm, respectively, as expected from the spectral intervals of Fig. 2. No measurable pulsation could be obtained in the case of a 20 μm-diameter SMRR, because only one microresonator mode would dominate in the central part of the amplifier bandwidth. For the other SMRR, as discussed below, the limited contrast of the autocorrelation traces can be attributed to two factors: the limited number of locked lines falling inside the amplifier bandwidth, and a remaining timing jitter. This anyway confirms the existence of partially mode-locked states, as in previous results using a similar hybrid cavity configuration [12, 15]. Moreover, in our experiment, by employing PM-fibers in the main cavity part, we could rule out the influence of nonlinear polarization evolution that is known to produce an effective ultrafast saturable absorber effect in presence of polarizing elements.

Let us discuss further the peculiar features of the observed dynamics. Figures 3 (b) and (c) show that the intensity pattern actually has a dual periodicity. This suggests that a secondary pulse of lower amplitude is generated in the microring cavity, and is located symmetrically on the microring. The spectra from Fig. 2 (a) for the 100 and 200 μm SMRR support this interpretation with the presence of stronger side comb lines. This repetition rate doubling behavior could either be explained by a technological imperfection leading to a preferred transmission of alternating modes of the SMRR, or by a dynamic pulse splitting within the SMRR cavity, due to the

intense effective nonlinearity at high amplifier gain. The contrast of the autocorrelation trace increases with the size of the SMRR. Indeed, assuming that the gain bandwidth and the pulse duration remain approximately the same for various SMRRs, the larger the number of SMRR lines, the larger the temporal spacing between successive pulses, and the better the autocorrelation contrast.

On Fig. 4, we show a side-by-side comparison between the 200 μm SMRR and the 50 μm SMRR spectral and temporal features. The autocorrelation traces were taken on a larger delay window, and show that the number of cross-correlation peaks is actually finite. This can be interpreted as a result of timing jitter, with the laser generating bunches of a few tens of coherent pulses at a time. A larger SMRR diameter tends to produce a longer coherence length, and a smaller duty cycle (individual pulse duration multiplied by the RF) that results in higher contrast. Pumping power increase also leads to an increase of the contrast and of the coherence time, as shown on Fig. 4.

Another noteworthy dynamical feature is the observation of a significant broadening of the lasing microring modes, as displayed on Fig. 2(b). With Q-factors higher than 10^5, the linewidth of the modes was indeed expected to be below 0.1 nm, in contradiction with the recorded spectra. The shape of this broadening is in fact consistent with a self-phase-modulation induced nonlinear broadening within the highly nonlinear SOI waveguides. This broadening can either appear in the silica fiber, after the amplifier where the power is maximum, or within the waveguide, after the resonator has filtered the modes to its linewidth. In the first case, a nonlinear phase shift of one radian would require a peak power of $P_p = 1/(\gamma_0 L_0)$, where $L_0 \simeq 10\,\mathrm{m}$ and comprises the EDFA length. This calculation yields a value of 100 W for the pulses' peak power. In contrast, the same nonlinear phase shift is obtained with a peak power of 2.6 W in 1 mm of SOI waveguide, a much lower value. Therefore, we attribute the main spectral broadening to the SMRR, which is consistent with the interpretation of [12, 13], which gives the microresonator a full role of both spectral selection and four-wave mixing, mechanisms that can lead to laser mode locking.

4. CONCLUSION

In summary, we have inserted a SOI microring resonator in a fiber laser. By ruling out the influence of nonlinear polarization mode locking in our laser architecture, we checked that the SOI microring had the attributes of a mode-locking element, allowing to generate pulse trains at very high repetition rates ranging from 110 GHz to 450 GHz. Whereas only partial mode locking was obtained, we demonstrated that the coherence of the pulse trains increased with the diameter of the microring resonator, which is a logical consequence of the increase of both finesse and nonlinearity of the

microring with an increased diameter. More surprising, was the observation that the microring could support the generation of pulse trains with a repetition frequency that was the double of the microring free spectral range. Finally, we noticed that the ultrafast pulse train was powerful enough to generate a significant nonlinear broadening of the comb lines in the output waveguide. Our experimental investigation brings interesting perspectives concerning the coupling-efficient embedding of silicon integrated devices into fiber cavities, and pave the way for experiments at higher wavelengths, above the two-photon absorption bandgap.

Acknowledgements. This work has been supported by the Labex ACTION (contract ANR-11-LABX-0001-01) and CEFIPRA programs (project 5104-2).

REFERENCES

1. D. Cotter *et al.*, Science **286** (5444), 1523–1528 (1999).
2. T. R. Schibli *et al.*, Opt. Lett. **29** (21), 2467–2469 (2004).
3. N. R. Newbury and W. C. Swann, J. Opt. Soc. Am. B **24** (8), 1756–1770 (2007).
4. K. Merghem *et al.*, Appl. Phys. Lett. **94** (2), 021107 (2009).
5. T. F. Carruthers and I. N. Duling, Opt. Lett. **21** (23), 1927–1929 (1996).
6. A. B. Grudinin and S. Gray, J. Opt. Soc. Am. B **14** (1), 144–154 (1997).
7. C. Lecaplain and P. Grelu, Opt. Express **21** (9), 10897–10902 (2013).
8. P. Franco *et al.*, Opt. Lett. **20** (19), 2009–2011 (1995).
9. E. Yoshida and M. Nakazawa, Opt. Lett. **22** (18), 1409–1411 (1997).
10. D. Mao, X. Liu, Z. Sun, H. Lu, D. Han, G. Wang, and F. Wang, Sci. Rep. **3**, 3223 (2013).
11. R. Si Fodil, F. Amrani, C. Yang, A. Kellou, and P. Grelu, Phys. Rev. A **94**, 013813 (2016).
12. M. Peccianti *et al.*, Nature Commun. **3**, 765 (2012).
13. A. Pasquazi *et al.*, Opt. Express **20** (24), 27355–27363 (2012).
14. L.-G. Yang *et al.*, Laser Phys. Lett. **11** (6), 065101 (2014).
15. Y. Liu *et al.*, Laser Phys. Lett. **13** (3), 035101 (2016).
16. R. Soref, IEEE Journal Select. Top. Quantum Electron. **12** (6), 1678–1687 (2006).
17. M. Lipson, J. Lightwave Techn. **23** (12), 4222–4238 (2005).
18. J. Leuthold, C. Koos, and W. Freude, Nature Photon. **4** (8), 535–544 (2010).
19. M. Hofer *et al.*, IEEE J. Quantum Electron. **28** (3), 720–728 (1992).
20. I. Märki *et al.*, J. Appl. Phys. **98** (1), 013103 (2005).
21. D. Taillaert *et al.*, IEEE J. Quantum Electron. **38** (7), 949–955 (2002).
22. F. Koch, S. Chernikov, and J.R. Taylor, Opt. Commun. **175**, 209–213 (2000).
23. H. Tsang and Y. Liu, Semiconductor Science and Technology **23** (6), 064007 (2008).
24. A. C. Turner-Foster *et al.*, Opt. Express **18** (4), 3582–3591 (2010).
25. G. Priem *et al.*, Opt. Express **13** (23), 9623–9628 (2005).
26. Q. Xu and M. Lipson, Opt. Lett. **31** (3), 341–343 (2006).
27. Q. Lin, O. J. Painter, and G. P. Agrawal, Opt. Express **15** (25), 16604–16644 (2007).
28. O. Boyraz, T. Indukuri, and B. Jalali, Opt. Express **12** (5), 829–834 (2004).
29. V. R. Almeida *et al.*, Nature **431** (7012), 1081–1084 (2004).